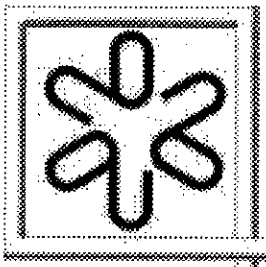

Instituto de Física
Universidade de São Paulo

Probing the LSND mass scale and four neutrino scenarios with a neutrino telescope

Nunokawa, H., Peres, O.L.G. and Funchal, R. Zukanovich

Publicação IF – 1567/2003

UNIVERSIDADE DE SÃO PAULO
Instituto de Física
Caixa Postal 66.318
05315-970 - São Paulo - Brasil

IFT-P.007/2003
IFUSP-DFN/03-079
NSF-ITP-03-09
hep-ph/0302039

Probing the LSND mass scale and four neutrino scenarios with a neutrino telescope

H. Nunokawa[1,2,*] O. L. G. Peres[2,3,†] and R. Zukanovich Funchal[2,4‡]
[1] *Instituto de Física Teórica, Universidade Estadual Paulista, Rua Pamplona 145, 01405-900 São Paulo, Brazil*
[2] *Kavli Institute for Theoretical Physics, University of California, Santa Barbara, CA 93106, USA*
[3] *Instituto de Física Gleb Wataghin, Universidade Estadual de Campinas - UNICAMP, 13083-970 Campinas, Brazil*
[4] *Instituto de Física, Universidade de São Paulo C. P. 66.318, 05315-970 São Paulo, Brazil*
(Dated: April 25, 2003)

We show in this paper that the observation of the angular distribution of upward-going muons and cascade events induced by atmospheric neutrinos at the TeV energy scale, which can be performed by a kilometer-scale neutrino telescope, such as the IceCube detector, can be used to probe a large neutrino mass splitting, $|\Delta m^2| \sim (0.5-2.0)$ eV^2, implied by the LSND experiment and discriminate among four neutrino mass schemes. This is due to the fact that such a large mass scale can promote non negligible $\nu_\mu \to \nu_e, \nu_\tau/\bar{\nu}_\mu \to \bar{\nu}_e, \bar{\nu}_\tau$ conversions at these energies by the MSW effect as well as vacuum oscillation, unlike what is expected if all the neutrino mass splittings are small.

PACS numbers: 14.60.St,14.60.Pq,14.60.Lm,95.55.Vj,95.85.Ry.

I. INTRODUCTION

Atmospheric and solar neutrino experiments present today compelling evidence of neutrino flavor oscillations induced, respectively, by the mass squared differences $|\Delta m^2_{\rm ATM}| \sim 3 \times 10^{-3}$ eV^2 [1] and $\Delta m^2_\odot \sim 7 \times 10^{-5}$ eV^2 [2]. These results have been independently supported by the K2K experiment [3], confirming the $\nu_\mu/\bar{\nu}_\mu$ conversion observed in atmospheric neutrino data, and by the KamLAND experiment [4], recently observing $\bar{\nu}_e$ disappearance compatible with what has been seen by the solar neutrino experiments.

In the standard three neutrino flavor oscillation framework, the above results imply neutrino oscillation lengths at energies above about 0.3 TeV much greater than the Earth's diameter, strongly suppressing $\nu_\mu \to \nu_e/\nu_\tau$ and $\bar{\nu}_\mu \to \bar{\nu}_e/\bar{\nu}_\tau$ oscillations. Moreover, the ratio between $\nu_e/\bar{\nu}_e$ and $\nu_\mu/\bar{\nu}_\mu$ atmospheric fluxes drops as their energy increases so that atmospheric neutrino data above 0.5 TeV are expected to be basically composed of ν_μ and $\bar{\nu}_\mu$ [5]. The so called prompt atmospheric neutrinos coming from the decay of charmed particles as well as extra-galactic $\nu_e, \bar{\nu}_e/\nu_\tau, \bar{\nu}_\tau$ contributions are very small compared to the conventional atmospheric $\nu_\mu/\bar{\nu}_\mu$ fluxes (which mainly come from the decay of charged pions and kaons) in the 0.5-10 TeV energy range [6].

However, as we will see, atmospheric $\nu_e, \bar{\nu}_e/\nu_\tau, \bar{\nu}_\tau$ fluxes in the TeV energy range can be non-negligible compared to the $\nu_\mu/\bar{\nu}_\mu$ if the result of LSND experiment [7] which indicates $\bar{\nu}_\mu \to \bar{\nu}_e$ transition generated by neutrino oscillations with a large mass scale, $|\Delta m^2_{\rm LSND}| \sim (0.5-2.0)$ eV^2, turns out to be correct. The LSND result, which will be very soon tested by the MiniBooNE experiment [8], if confirmed, can be interpreted in combination with the atmospheric and solar neutrino data as a signature of an additional neutrino, ν_s, sterile in nature. The minimum scheme necessary to explain at same time all three indications of neutrino oscillations involves four neutrino mass eigenstates [9]. We are aware that current analyses performed with the entire set of neutrino data from accelerators, reactors, solar and atmospheric neutrinos seem to disfavor four neutrino mass scenarios [10, 11]. See, however, Refs. [12] which casted doubt on conclusions drawn in Refs. [10, 11]. More importantly, no experiment until now has confirmed or ruled out the LSND result and one should wait for results from MiniBooNE.

We will show in this letter that in the framework of four neutrino mass schemes, atmospheric neutrino data at the TeV energy scale may contain a non negligible amount of ν_e or $\bar{\nu}_e$, due to the interplay of the Earth matter with the LSND mass scale through the so called MSW effect [13], and of ν_τ and $\bar{\nu}_\tau$, due to almost vacuum oscillations induced by this same mass scale. To our knowledge it has been never mentioned before in the literature that the LSND mass

*Electronic address: nunokawa@ift.unesp.br
†Electronic address: orlando@ifi.unicamp.br
‡Electronic address: zukanov@if.usp.br

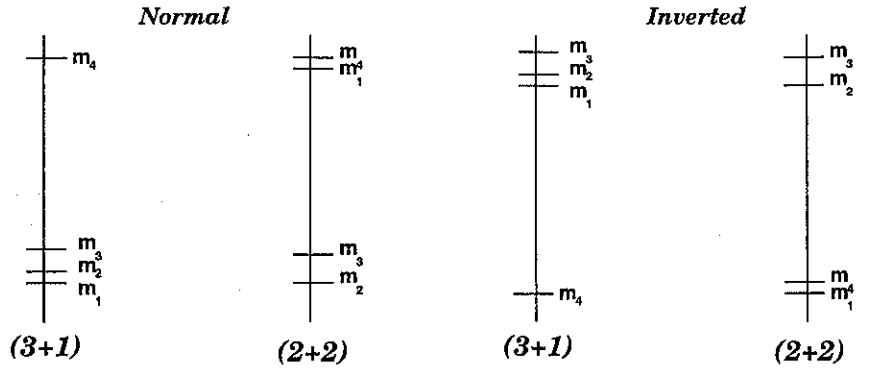

FIG. 1: Four neutrino mass schemes used in this paper.

splitting could give rise to resonant $\nu_\mu \to \nu_e$ or $\bar{\nu}_\mu \to \bar{\nu}_e$ conversion for atmospheric neutrinos. These $\nu_e, \bar{\nu}_e/\nu_\tau, \bar{\nu}_\tau$ events can be observed by a large neutrino telescope, such as the proposed IceCube detector [14], by measuring the angular distribution of upward-going muons and cascade events. This is because the zenithal dependence of upward-going muons as well as of cascade events will be modified by these new contributions with respect to what would be expected for the standard three neutrino oscillation framework. The zenithal distortions can not only discriminate among the different types of four neutrino mass schemes, but also they are sensitive to the sign of the LSND mass splitting, opening a new window to test four neutrino mass scenarios.

II. FRAMEWORK OF FOUR NEUTRINO MIXING SCHEMES

We will work in the minimal model structure needed to describe the three evidence for neutrino oscillations (atmospheric, solar and LSND): a four neutrino mass scheme [9]. We will adopt the same parametrization and some useful notations used in Refs [10, 15]. For what concerns us here, the sign of $\Delta m^2_\odot$ and of $\Delta m^2_{\rm ATM}$ are irrelevant, only the sign of $\Delta m^2_{\rm LSND}$ will be significant. We can then classify the possible four neutrino mass schemes into two categories: (a) *(3+1)*, when a single neutrino mass state is separated from the other neutrino mass states by a large mass splitting ($|\Delta m^2_{\rm LSND}|$); and (b) *(2+2)*, when two pairs of neutrino mass states are separated by a gap given by the $|\Delta m^2_{\rm LSND}|$ scale. Moreover, when ν_4 is a heavy (light) state we will call it normal (inverted) mass hierarchy. We show in Fig. 1, the *(2+2)* and *(3+1)* mass schemes for both, normal and inverted, mass hierarchies which will be considered in this paper.

The evolution equations for neutrinos in the flavor basis are

$$i\frac{d}{dr}\nu_f = \left[U\frac{M^2}{2E_\nu}U^T + A\right]\nu_f, \tag{1}$$

where $\nu_f = (\nu_e\nu_\mu\nu_\tau\nu_s)^T$ and E_ν is the neutrino energy. We define $\Delta m^2_{\rm LSND} = \Delta m^2_{42}$ and $\Delta m^2_{\rm ATM} = \Delta m^2_{32}$, with $\Delta m^2_{ij} = m^2_i - m^2_j$, for $i, j = 1, 2, 3, 4$. The diagonalized neutrino mass squared matrix is

$$M^2 = \mathrm{diag}(0, -\Delta\mathrm{m}^2_{\rm LSND} + \Delta\mathrm{m}^2_\odot, \Delta\mathrm{m}^2_{\rm ATM} + \Delta\mathrm{m}^2_\odot - \Delta\mathrm{m}^2_{\rm LSND}, \Delta\mathrm{m}^2_\odot), \tag{2}$$

with $\Delta m^2_\odot = \Delta m^2_{41}$ for $(2+2)$ cases and

$$M^2 = \mathrm{diag}(0, \Delta\mathrm{m}^2_\odot, \Delta\mathrm{m}^2_\odot + \Delta\mathrm{m}^2_{\rm ATM}, \Delta\mathrm{m}^2_{\rm LSND} + \Delta\mathrm{m}^2_\odot), \tag{3}$$

with $\Delta m^2_\odot = \Delta m^2_{21}$ for $(3+1)$ ones. We use for the 4×4 mixing matrix U the same parametrization as in Ref. [15],

$$U = R_{34}R_{24}R_{23}R_{14}R_{13}R_{12}, \tag{4}$$

where R_{ij} are rotation matrices in the subspace (i, j) with angle θ_{ij}. The matter potential matrix is

$$A = \mathrm{diag}(\mathrm{A_{cc}}, 0, 0, \mathrm{A_{nc}}), \tag{5}$$

with $A_{\rm cc} = \sqrt{2}G_F\rho Y_e$ and $A_{\rm nc} = A_{\rm cc}(1-Y_e)/(2Y_e)$, where G_F is the Fermi constant, Y_e the electron fraction and ρ the matter density. For antineutrinos evolution equations similar to Eq. (1) exist but with $A \to -A$. We have ignored all CP violation phases, as they do not play any important rôle in our study.

In order to make clear the connection among mixing parameters and experimental observations, we will introduce some useful definitions. Let us first define the quantities d_α ($\alpha = e, \mu, \tau, s$) as

$$d_\alpha = \begin{cases} |U_{\alpha 4}|^2 & \text{for } (3{+}1) \text{ mass scheme,} \\ |U_{\alpha 1}|^2 + |U_{\alpha 4}|^2 & \text{for } (2{+}2) \text{ mass scheme,} \end{cases} \tag{6}$$

and η_α ($\alpha = e, \mu, \tau, s$) as

$$\eta_\alpha = \begin{cases} |U_{\alpha 1}|^2 + |U_{\alpha 2}|^2 & \text{for } (3{+}1) \text{ mass scheme,} \\ |U_{\alpha 1}|^2 + |U_{\alpha 4}|^2 & \text{for } (2{+}2) \text{ mass scheme,} \end{cases} \tag{7}$$

which can be related to the neutrino survival and oscillation probabilities at short and long-baseline experiments as we will see below.

Note that η_s measures the sterile admixture in solar neutrino oscillations, this parameter describes the fraction of sterile neutrino participating in solar oscillations: $\eta_s = 0$ (1) corresponds to pure active (sterile) $\nu_e \to \nu_\tau$ ($\nu_e \to \nu_s$) oscillations. Solar neutrino data prefer a small admixture of sterile neutrino in the $\Delta m^2_\odot$ scale, *i.e.*, $\eta_s \ll 1$. The sterile admixture for atmospheric neutrinos is characterized by the parameter d_s, in the $\Delta m^2_{\rm ATM}$ mass scale, $d_s = 1$ (0) corresponds to pure active (sterile) $\nu_\mu \to \nu_\tau$ ($\nu_\mu \to \nu_s$) oscillations. Atmospheric neutrino data prefer a small admixture of sterile neutrino in the $\Delta m^2_{\rm ATM}$ scale, *i.e.*, $1 - d_s \ll 1$.

We can relate d_α to the neutrino survival probability in vacuum for short-baseline disappearance experiments, ignoring $\mathcal{O}(\Delta m^2_{\rm ATM})$ corrections, by

$$P_{\nu_\alpha \to \nu_\alpha} = 1 - A_{\alpha;\alpha} \sin^2\left(\frac{\Delta m^2_{\rm LSND}}{4E_\nu} L\right) = 1 - 4\, d_\alpha (1 - d_\alpha) \sin^2\left(\frac{\Delta m^2_{\rm LSND}}{4E_\nu} L\right), \tag{8}$$

where L is the baseline distance. From the null results of short-baseline experiments $A_{e;e}$ and $A_{\mu;\mu}$ are limited to be very small [9].

The conversion probability, relevant for short-baseline appearance experiments, can be written as

$$P_{\nu_\mu \to \nu_e} = A_{\mu;e} \sin^2\left(\frac{\Delta m^2_{\rm LSND}}{4E_\nu} L\right), \tag{9}$$

where

$$A_{\mu;e} = \begin{cases} 4|U_{e4}|^2 |U_{\mu 4}|^2 & \text{for } (3{+}1) \text{ mass scheme,} \\ 4|U_{e1} U^*_{\mu 1} + U_{e4} U^*_{\mu 4}|^2 & \text{for } (2{+}2) \text{ mass scheme.} \end{cases} \tag{10}$$

Here the amplitude $A_{\mu;e}$ can be identified as the LSND mixing amplitude $\sin^2 2\theta_{\rm LSND}$ [7].

For the long-baseline reactor ($L \lesssim 1$ km) and accelerator experiments ($L < 1000$ km), we have to include effects of the $\Delta m^2_{\rm ATM}$ mass scale, and the conversion probability, $P^{\rm CH}_{\nu_\mu \to \nu_e}$ becomes

$$P^{\rm CH}_{\nu_\mu \to \nu_e} = 1 - 2\, d_e (1 - d_e) - A_{\rm CH} \sin^2\left(\frac{\Delta m^2_{\rm ATM}}{4E_\nu} L\right), \tag{11}$$

with

$$A_{\rm CH} = \begin{cases} 4\, \eta_e (1 - d_e - \eta_e) & \text{for } (3{+}1) \text{ mass scheme,} \\ 4\, |U_{e2}|^2 |U_{e3}|^2 & \text{for } (2{+}2) \text{ mass scheme.} \end{cases} \tag{12}$$

To accommodate the (*2+2*) mass scheme, d_μ, $A_{\rm CH}$ and $A_{\mu;e}$ have to be small and d_e close to 1 (to keep $A_{e;e}$ amplitude small). Also the parameters η_s and d_s are not independent, $\eta_s = d_s$ as noted by the authors of Ref. [16]. From Ref.[15] we know that the global fit of atmospheric and solar neutrino data prefers either the limit $\eta_s = d_s \sim 1$ or the limit $\eta_s = d_s \ll 1$. For the (*3+1*) mass scheme, d_μ,d_e, $A_{\rm CH}$, $A_{\mu;e}$, η_s and $1 - d_s$, all, have to be small

In this paper, in order to give an explicit example of the effect of four neutrino mass schemes we will fix the values of the mixing parameters. These were taken within the parameter region allowed by solar and atmospheric neutrino data as well as by the null results of reactors and accelerators (with the exceptions of K2K [3] and KamLAND [4]) [1, 9]. We have scanned a grid of values to find the maximal possible values of the six mixing angles in order to maximize the oscillation effect driven by the LSND mass scale in IceCube, using the constraints on d_α, $A_{\mu;e}$, $A_{\rm CH}$, η_e and η_s

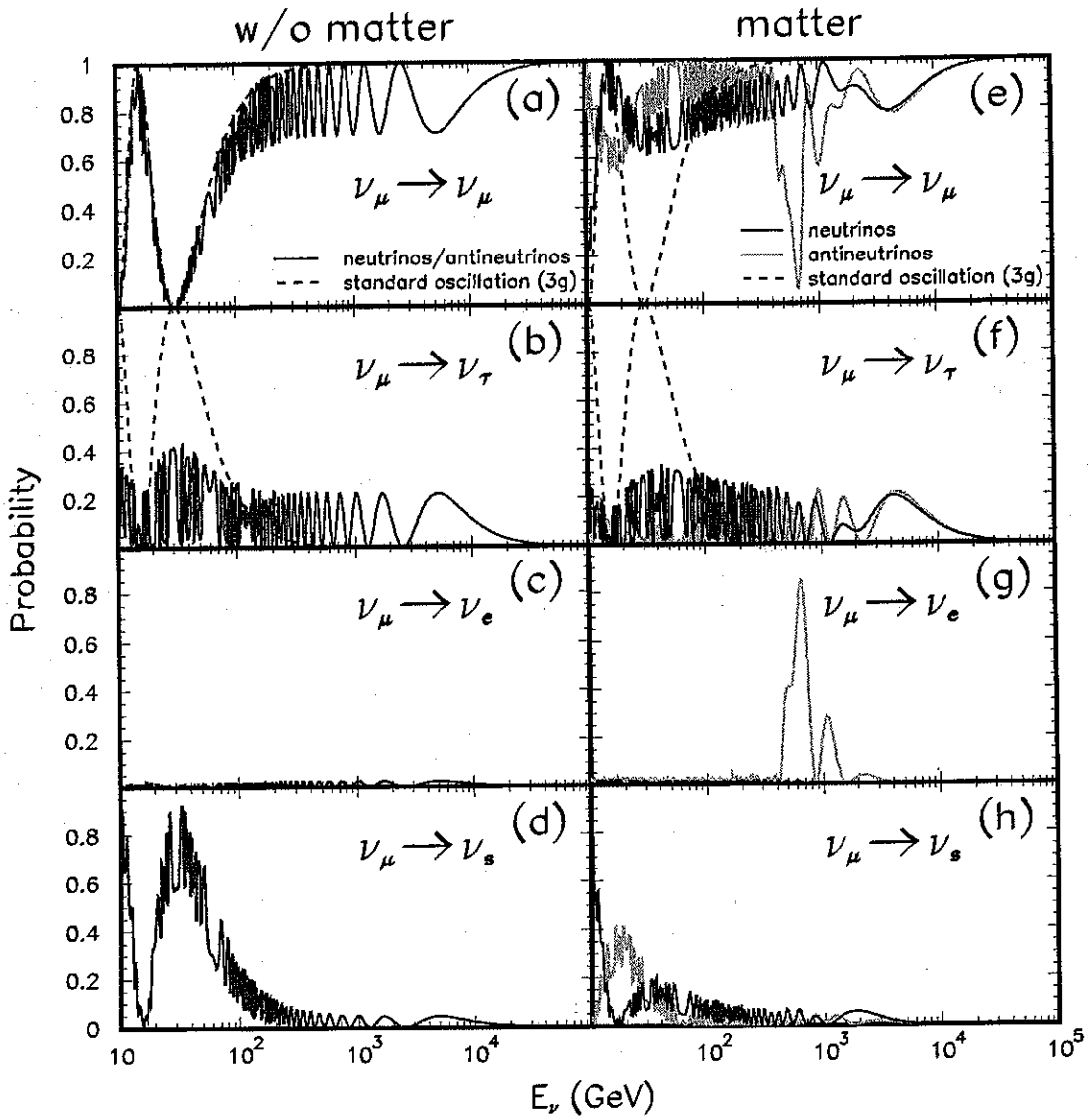

FIG. 2: Neutrino and anti-neutrino probabilities, for diametral trajectories ($\cos\theta_z = -1$), in the *(2+2)* scheme with normal hierarchy for $\Delta m^2_{\rm LSND} = 0.5$ eV^2 *without* (left panels) and *with* (right panels) matter effects taken into account. We have used $\Delta m^2_{\rm ATM} = 3 \times 10^{-3}$ eV^2, $\Delta m^2_{\odot} = 7 \times 10^{-5}$eV^2 and the mixing parameter as given in Table I. The standard three generation oscillation probabilities are labeled as 3(g).

shown in Ref. [15]. The result of our scan is shown in Table I. For the neutrino mass splittings, we have used the best fit values $\Delta m^2_{\rm ATM} = 3 \times 10^{-3}$ eV^2 and $\Delta m^2_{\odot} = 7 \times 10^{-5}$ eV^2. For definiteness we also have set $|\Delta m^2_{\rm LSND}| = 0.5$ eV^2.

We have numerically solved Eq. (1) to compute $P(\nu_\mu \to \nu_\alpha)$ for $\alpha = e, \mu, \tau$ and s, the oscillation probabilities that are relevant for atmospheric neutrino data. Let us make some observations that can help the reader to understand our numerical results.

(2+2) case:

From the expressions of the evolution equations, one can expect matter enhanced MSW resonant conversion in Earth for the neutrino (antineutrino) channel $\nu_\mu \to \nu_e$ ($\bar\nu_\mu \to \bar\nu_e$), for the *2+2* inverted (normal) hierarchy if the

Case	$\sin^2\theta_{12}$	$\sin^2\theta_{13}$	$\sin^2\theta_{14}$	$\sin^2\theta_{34}$	$\sin^2\theta_{24}$	$\sin^2\theta_{23}$	η_s	d_s
2+2	0.001	0.01	0.26	0.8	0.03	0.5	0.2	0.2
3+1	0.26	0.035	0.02	0.45	0.045	0.5	0.13	0.52

TABLE I: Values of the mixing parameters used in this paper.

following condition is satisfied,

$$E_\nu^{\rm R} \sim |\Delta m^2_{\rm LSND}| \times \frac{d_e - d_\mu}{2A_{\rm cc}} \sim 1.7\ {\rm TeV} \times (d_e - d_\mu) \times \left(\frac{|\Delta m^2_{\rm LSND}|}{0.5\,{\rm eV}^2}\right) \times \left(\frac{2.0\,{\rm g/cc}}{Y_e\rho}\right). \tag{13}$$

Other resonances can be induced by the $\Delta m^2_{\rm ATM}$ mass scale at $E_\nu \lesssim 100$ GeV, but they are irrelevant for our purpose here. In the *(2+2)* mass scheme, $d_e \sim 1$ and $d_\mu \ll 1$ so that the resonant condition can be achieved in the TeV energy range. For the $\nu_\mu \to \nu_\tau$ channel we expect almost vacuum oscillations.

In Fig. 2 we show, for diametral trajectories ($\cos\theta_z = -1$), the behavior of the neutrino and antineutrino $\nu_\mu \to \nu_\mu$ and $\nu_\mu \to \nu_\tau, \nu_e, \nu_s$ transition probabilities for the *(2+2)* case with normal hierarchy. To provide a better understanding of what is going on, in panels (a)-(d) the matter effects were not taken into account while in panels (e)-(h) they were. We also show for comparison what would be expected for the standard three flavor neutrino oscillation scenario (labeled as 3(g)).

If we compare Fig. 2(c) and Fig. 2(g), we see a sizable $\bar\nu_\mu \to \bar\nu_e$ conversion probability when matter effects are taken into account. This resonance behavior is due to the LSND mass scale and Earth matter effects [13]. Looking closely to Fig. 2(g), we can see three peaks: one at $E_\nu^{\rm R} \sim 0.57$ TeV for a typical value of Earth core density ($\rho_{\rm core} \sim 12$g/cc), and another for $E_\nu^{\rm R} \sim 1.5$ TeV for a typical value of Earth mantle density, ($\rho_{\rm mantle} \sim 4$g/cc). A third peak appears for $E_\nu^{\rm R} \sim 0.8$ TeV and its origin is due to a parametric resonance. Similar behavior was noticed sometime ago in the context of neutrino oscillations induced by $\Delta m^2_{\rm ATM}$ for $\nu_\mu \to \nu_s$ [17]. To determine the behavior of oscillations in $\nu_\mu \to \nu_\tau$ channel, we can use Eq. (9), changing $e \to \tau$, so that $P_{\nu_\mu \to \nu_\tau} = A_{\mu;\tau}\ \sin^2(\Delta m^2_{\rm LSND} L/(4E_\nu))$. The conversion amplitude for this channel, $A_{\mu;\tau} = 4\cos^2\theta_{34}\cos^2\theta_{24}\sin^2\theta_{24}$ depends only on $\sin^2\theta_{24}$ and $\sin^2\theta_{34}$. We confirmed numerically that this is correct and we have virtually vacuum oscillations induced by $\Delta m^2_{\rm LSND}$ as you can see comparing Figs. 2(b) and (f). In the case of inverted mass hierarchy, the neutrino and antineutrino probabilities are interchanged.

(3+1) case:

In the *(3+1)* mass scheme, we cannot expect a strong resonant $\nu_\mu \to \nu_e$ ($\bar\nu_\mu \to \bar\nu_e$) transition due to the LSND mass scale at TeV energies. This can be explained as follows. First, both ν_μ and ν_e ($\bar\nu_\mu$ and $\bar\nu_e$) are basically distributed among the mass triplet so that we cannot expect a significant direct transition between them driven by $\Delta m^2_{\rm LSND}$. However, a second order transition can be achieved via ν_4 which is mainly composed of ν_s as $\nu_\mu \to \nu_s \to \nu_e$ ($\bar\nu_\mu \to \bar\nu_s \to \bar\nu_e$).

For the normal mass hierarchy, the first step, $\nu_\mu \to \nu_s$ ($\bar\nu_\mu \to \bar\nu_s$), occurs via almost vacuum oscillation (a MSW resonance effect), while the second step, $\nu_s \to \nu_e$ ($\bar\nu_s \to \bar\nu_e$), occurs via a MSW resonance effect with $E_\nu^{\rm R}$ given by Eq. (13) with $d_e - d_\mu$ replaced by d_s (almost vacuum oscillation). The strength of these transitions is regulated by the value of θ_{14} and θ_{24}, which are very much constrained by current data (see Table I). This is why we do not expect to observe a large number of ν_e ($\bar\nu_e$) events in the *(3+1)* scheme. In the case of inverted mass hierarchy, the neutrino and antineutrino probabilities are interchanged.

On the other hand, $\nu_\mu \to \nu_\tau$ ($\bar\nu_\mu \to \bar\nu_\tau$) transitions driven by the LSND mass scale can occur directly mainly via vacuum-like oscillation, since there is a significant amount of ν_τ in the ν_4 state. This is due to the large value of θ_{34} (see Table I), which is the maximal value still allowed by data.

These observations are confirmed by our numerical calculations. In Fig. 3 we show, for diametral trajectories ($\cos\theta_z = -1$), the behavior of the neutrino and antineutrino $\nu_\mu \to \nu_\mu$ and $\nu_\mu \to \nu_\tau, \nu_e, \nu_s$ transition probabilities for the *(3+1)* case with normal hierarchy in a similar way as in Fig. 2.

From these observations we should expect at the TeV energy scale $\nu_\mu \to \nu_e$ matter enhanced resonant transitions for neutrinos (antineutrinos) if the LSND mass hierarchy is normal (inverted) in the *(2+2)* scheme and $\nu_\mu \to \nu_\tau$ as well as $\bar\nu_\mu \to \bar\nu_\tau$ vacuum-like transitions in both mass schemes.

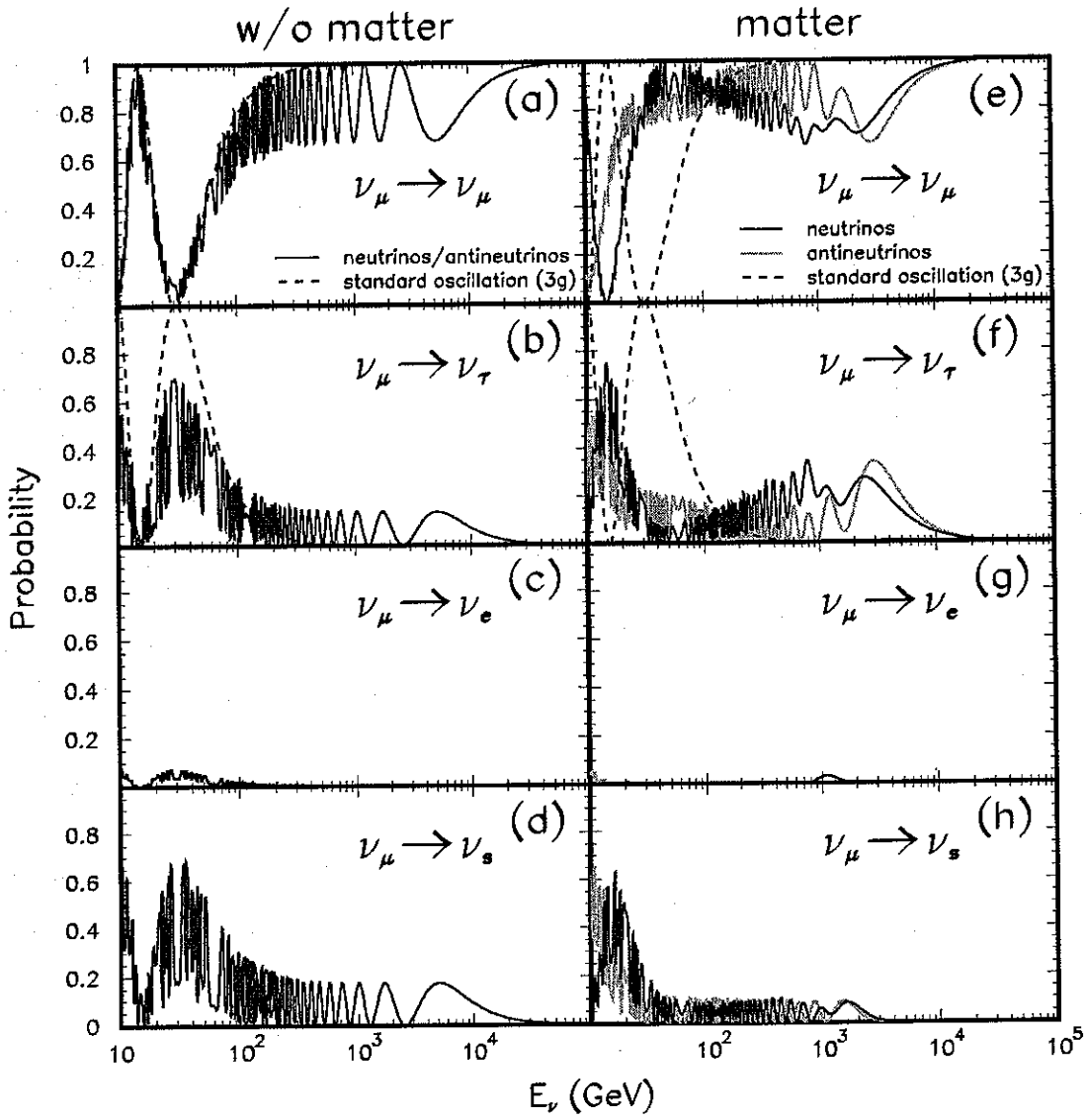

FIG. 3: Neutrino and anti-neutrino probabilities, for diametral trajectories ($\cos\theta_z = -1$), in the *(3+1)* scheme with normal hierarchy for $\Delta m^2_{\rm LSND} = 0.5$ eV^2 *without* (left panels) and *with* (right panels) matter effects taken into account. We have used $\Delta m^2_{\rm ATM} = 3 \times 10^{-3}$ eV^2, $\Delta m^2_{\odot} = 7 \times 10^{-5}$eV^2 and the mixing parameter as given in Table I. The standard three generation oscillation probabilities are labeled as 3(g).

III. TYPES OF SIGNAL EVENTS

We have studied the observable consequences of these four neutrino schemes at high energies, in a future neutrino telescope. For definiteness we have assumed a kilometer-scale neutrino telescope as the one proposed by the IceCube collaboration [14] that, for simplicity, has been simulated with perfect efficiency as well as perfect angular and energy resolution. We have supposed that the IceCube detector can be described by a cylinder with 900 m of height and 500 m radius.

We have calculated two types of measurable signals in this detector: upward-going muons and cascades events. The calculations were done using the atmospheric neutrino fluxes, denoted by Φ_{ν_α}, $\alpha = e, \mu$, of the Bartol group [18] and the cross sections from Ref. [19]. We have also included in our calculations the effect of neutrino absorption when crossing the Earth, taking from Ref. [19].

A. Upward-going muons

Muon neutrino charged current interactions, occurring inside the Earth close enough to the detector, may produce energetic muon events which can cross the detector volume, giving rise to the so-called upward-going muons. These events are characterized by a very good angular resolution.

We have calculated the number of upward-going muon events as a function of the zenith angle, $N_\mu(\theta_z)$, as in Refs. [20, 21],

$$N_\mu(\theta_z) = T \int_{E_{\mu,\min}}^{\infty} A(R_{\min}, \theta_z) \frac{d\Phi_\mu(E_\mu, \cos\theta_z)}{dE_\mu d\cos\theta_z} dE_\mu + \text{antineutrinos}, \tag{14}$$

with

$$\begin{aligned} \frac{d\Phi_\mu}{dE_\mu d\cos\theta_z} &= N_A \int_{E_\mu}^{\infty} dE_{\mu 0} \int_{E_{\mu 0}}^{\infty} dE_\nu \int_0^{\infty} dh\, \kappa_{\nu_\mu}(h, \cos\theta_z, E_\nu) \\ &\times \frac{d\Phi_{\nu_\mu}(E_\nu, \theta_z)}{dE_\nu d\cos\theta_z} P(\nu_\mu \to \nu_\mu) \frac{d\sigma(E_\nu, E_{\mu 0})}{dE_{\mu 0}} F_{\text{rock}}(E_{\mu 0}, E_\mu) S(E_\nu, \theta_z), \end{aligned} \tag{15}$$

where T is the livetime that we assumed to be 1 yr, N_A is the Avogadro number, $E_{\mu 0}$ is the energy of the muon produced in the neutrino interaction and E_μ is the muon energy when entering the detector, $F_{\text{rock}}(E_{\mu 0}, E_\mu)$ is a function that takes into account the muon energy loss from the point where the muon is created to where it is detected [20], κ_α is the slant distance distribution normalized to one [22], $P(\nu_\mu \to \nu_\mu)$ is the muon survival probability, $A(R_{\min}, \theta_z)$ is the effective area for a muon traveling a distance $R_{\min}$ inside the detector coming from the direction θ_z [20], σ is the $\nu_\mu N \to \mu X$, neutrino cross section, $\cos\theta_z$ labels both the neutrino and the muon directions which to a very good approximation at the relevant energies are collinear, $S(E_\nu, \theta_z)$ is a shadow factor that is related to the attenuation of neutrinos traversing the Earth [19]. For a given zenith angle, the threshold energy cut is obtained by equating $R(E_{\mu,\min}) = R_{\min} = 100$ m, where $R(E_{\mu,\min})$ is the muon range function.

In Fig. 4 we show the zenithal angle distribution of these events expected in the case of the standard three flavor oscillations (or no oscillations at all) and for each of the four neutrino mass schemes assuming $|\Delta m^2_{\text{LSND}}| = 0.5\ \text{eV}^2$ and the oscillation parameters as given in Table I. It is clear from this plot that the distribution of upward-going muons reflects the $\nu_\mu/\bar{\nu}_\mu$ disappearance into other flavors promoted by each of the four neutrino schemes, making them quite distinguishable from the standard three flavor oscillation case. It may be even possible to distinguish among *(2+2)* and *(3+1)* schemes, although their normal and inverted cases are virtually the same due to the fact that the mean energy of these events is much lower than the resonant energy ($E^{\text{R}}_\nu \sim 0.8$ TeV for $\Delta m^2_{\text{LSND}} = 0.5\ \text{eV}^2$). From the Eq. (14) we note that all muons with an energy sufficient high to travel a distance $R_{\min}$ are classified as upward-going muons, the original muon energy is integrated out so that the correlation between the original neutrino energy and the final muon energy is weak.

As a test of capability to discriminate the four neutrino mass schemes from the standard three generation oscillation we performed a simple χ^2 analysis, as follows. If we define $N^i_\mu(4\nu)$ ($N^i_\mu(3g)$) as the number of upward-going muons in the i-th zenith angle bin in four neutrino mass schemes (standard three neutrino mass scheme) showed in Fig. 4, then we can compute the function

$$\chi^2 = \sum_{i=1,20} \frac{(\eta\, N^i_\mu(4\nu) - N^i_\mu(3g))^2}{(\sigma^i_{(4\nu)} + \sigma^i_{(3g)})^2}, \tag{16}$$

where $\sigma^i_{(4\nu)}$ ($\sigma^i_{(3g)}$) is the statistical error on $N^i_\mu(4\nu)$ ($N^i_\mu(3g)$), for simplicity we have ignored systematic uncertainties. The parameter η is a normalization factor. If we assumed predictions of upward going muons in standard three generation are the correct ones, then the only possible change is a global normalization factor. We scan the parameter η to look for the best fit and for any of neutrino mass schemes the minimum χ^2 is much higher then the degrees of freedom, 20-1 (20 points minus 1 normalization factor), with a goodness of fit well below 1%. Then we conclude that for the choice of mixing parameters in this paper, it is very likely that the zenith angular distribution of upward going muons is sufficient to be separated from the usual standard three neutrino oscillations. From this we can say that independent of which four neutrino mass scheme nature chooses, we can always have a distinctive zenith distortion in upward-going muons.

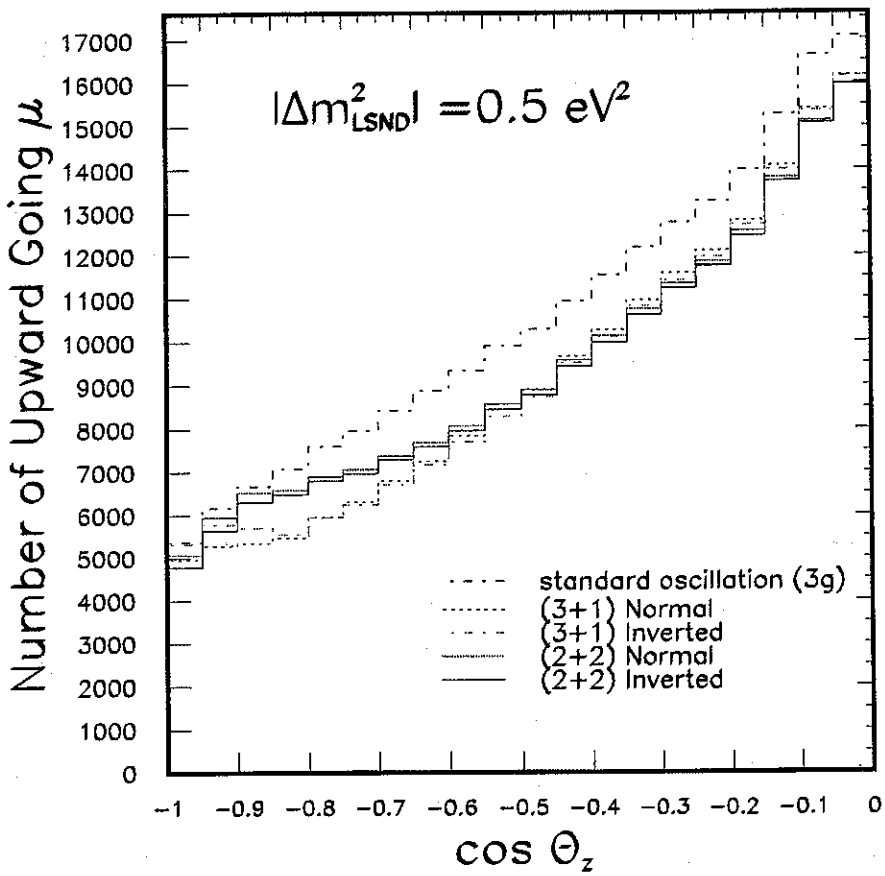

FIG. 4: Expected zenithal distribution of upward-going muon events in the IceCube experiment after one year of data taking for the standard three flavor oscillations (3g) and the different four neutrino mass schemes.

B. Cascades

Electromagnetic and hadronic showers can be produced by ionizing products of the neutrino interactions with the ice. These types of events can be created by electron neutrino charged current interactions (ν_e – CC), tau neutrino charged current interactions (ν_τ – CC) and neutral current interactions (ν – NC). These events, which are called cascade events, are characterized by a very good energy resolution. In principle, muon neutrinos also produce a hadronic shower and a muon and this case contribute to cascade events. We assume events with a muon track always can be separated from the other cascade events and we will not include them in our computation. We have calculated the number of cascade events for a given zenith angle, $N_{\rm cascade}(\theta_z)$, as in Refs. [23, 24],

$$N_{\rm cascade}(\theta_z) = TVN_A \int_{E_{\rm shr,min}}^{\infty} \frac{d\Phi_{\nu_\mu}(E_\nu, \cos\theta_z)}{dE_\nu d\cos\theta_z} P(\nu_\mu \to \nu_e) \sum_i f_i(E_\nu) dE_\nu + \text{antineutrinos}, \tag{17}$$

here V is the IceCube experiment volume (1 km^3), $f_i(E_\nu, z)$, $i = \nu_e$−CC, ν_τ−CC (hadronic plus electromagnetic showers), ν−NC, are functions which depend on the interaction,

$$f_{\nu_e-\mathrm{CC}}(E_\nu) = \int dy \frac{d\sigma_{cc}(E_\nu, y)}{dy} \Theta(E_\nu - E_{\mathrm{shr,min}}), \qquad \text{for } \nu_e - \mathrm{CC}$$

$$f^1_{\nu_\tau-\mathrm{CC}}(E_\nu) = \int dy \int dz \frac{d\sigma_{cc}(E_\nu, y)}{dy} \frac{dn(E_\tau)}{dz} \Theta(E_\nu(y + (1-y)(1-z)) - E_{\mathrm{shr,min}}), \qquad \text{for } \nu_\tau - \mathrm{CC \ hadronic}$$

$$f^2_{\nu_\tau-\mathrm{CC}}(E_\nu) = \int dy \int dz' \frac{d\sigma_{cc}(E_\nu, y)}{dy} \frac{dn(E_\tau)}{dz'} \Theta(E_\nu(y + (1-y)z') - E_{\mathrm{shr,min}}), \qquad \text{for } \nu_\tau - \mathrm{CC \ electromagnetic}$$

$$f_{\nu-\mathrm{NC}}(E_\nu) = \int dy \frac{d\sigma_{nc}(E_\nu, y)}{dy} \Theta(E_\nu y - E_{\mathrm{shr,min}}), \qquad \text{for } \nu - \mathrm{NC}$$

where E_τ is the tau energy, y, z, z' are the original neutrino energy fractions carried by the relevant lepton/hadron at play, and we have considered only events which have a total shower energy greater than 500 GeV ($E_{\mathrm{shr,min}} = 500$ GeV).

For ν_τ−CC events we can have hadronic and electromagnetic cascades, respectively, from $\nu_\tau \to \tau \to e$ decay channel and from $\nu_\tau \to \tau \to h$, where h means any hadrons. For ν−NC (ν_e−CC) events we have respectively hadronic (electromagnetic) showers. The functions $dn(E_\tau)/dz$ and $dn(E_\tau)/dz'$ are given in Ref. [24]. Although we also integrate on the neutrino energy as for the upward-going muons computation, the average shower energy for this sample is more closely related to the average initial neutrino energy.

Since for the energies considered here ($E_\nu \gtrsim 1$ TeV), the atmospheric neutrino fluxes are basically composed of ν_μ and $\bar{\nu}_\mu$ [5] and according to the usual three neutrinos oscillation scenario electron and tau neutrino appearance are suppressed, therefore one generally expects that only the neutral current contribution can produce cascades at these energies. A possible exception to this would be perhaps charged current contributions induced by ν_e/ν_τ neutrinos emitted in microquasar jets [25], but these events are very well collimated with the source and can be easily separated from the atmospheric neutrino data. As we have shown earlier, in four neutrino schemes, electron and tau neutrino components will appear at these energies so that an increase on the number of cascade events should be expected.

We show in Fig. 5 the zenithal distribution of cascade events that can be expected in IceCube after one year of data taking, for the standard three neutrino oscillation case as well as for all the four neutrino schemes, assuming $|\Delta m^2_{\mathrm{LSND}}| = 0.5$ eV^2 and the oscillation parameters as given in Table I. All four neutrino cases, for these values of the parameters, can be distinguished from the standard case. We observe that there is an increase on the number of cascade events at $\cos\theta_z \sim -1$ for the *(2+2)* inverted scheme due to the resonant appearance of ν_e similar to what is shown in Fig. 2 (g) for $\bar{\nu}_e$. There is no such a prominent peak for the *(2+2)* normal scheme due to the fact that in this case the resonance is in the antineutrino channel (where one has a lower flux and smaller cross section). The increase of the number of cascade events in the *(3+1)* schemes is almost exclusively due to ν_τ appearance. In fact, the angular distribution of cascade events reflect the flavor content of the atmospheric neutrino flux as measured at the detector site.

We observe that cascade events are more effective in separating the mass hierarchy of four neutrino schemes than the upward-going muon events. This is not surprising since the 500 GeV energy cut imposed on the cascade showers selects events closer to the resonant energy where the effect of the large $|\Delta m^2_{\mathrm{LSND}}| = 0.5$ eV^2 is more sizable. For higher values of $|\Delta m^2_{\mathrm{LSND}}|$ the differences among the standard and the four neutrino oscillations distributions could be even larger than what we have shown in Figs. 4 and 5 if not for the fact the mixing angles are much more constrained by data for higher masses [15]. In any case the general behavior of the curves shown in this paper will still hold for $|\Delta m^2_{\mathrm{LSND}}|$ as high as 2.0 eV^2.

We note that unlike the case of upward-going muon events, cascade events can be observed also for $\cos\theta_z > 0$, which correspond to down-going events. For such events, for any four neutrino mass scheme we have considered here, we do not expect any significant deviation of the zenith angle distribution from what is expected in the standard three neutrino oscillation scheme. In the standard scheme, in good approximation, the zenith angle distribution is symmetric with respect to $\cos\theta_z = 0$. This is because of the fact that for down-going cascade events, there is no matter effect and the distance traveled by neutrinos is much smaller than the typical oscillation length expected for $|\Delta m^2_{\mathrm{LSND}}|$ scale and $E_\nu \sim 1$ TeV so that no significant $\nu_e, \bar{\nu}_e/\nu_\tau, \bar{\nu}_\tau$ induced events are expected. Therefore, by comparing the zenith distributions for $\cos\theta_z > 0$ and $\cos\theta_z < 0$, it is expected that we can discriminate four neutrino mass schemes from the standard three one with better sensitivity.

Finally, let us note that the uncertainty in the prediction of the atmospheric muon neutrino flux, which is currently about 15%, could potentially spoil the discriminating power among the different signals. This can be, to some extent, overcome by combining cascade and upward-going muon events, and so reducing the uncertainty in the overall flux.

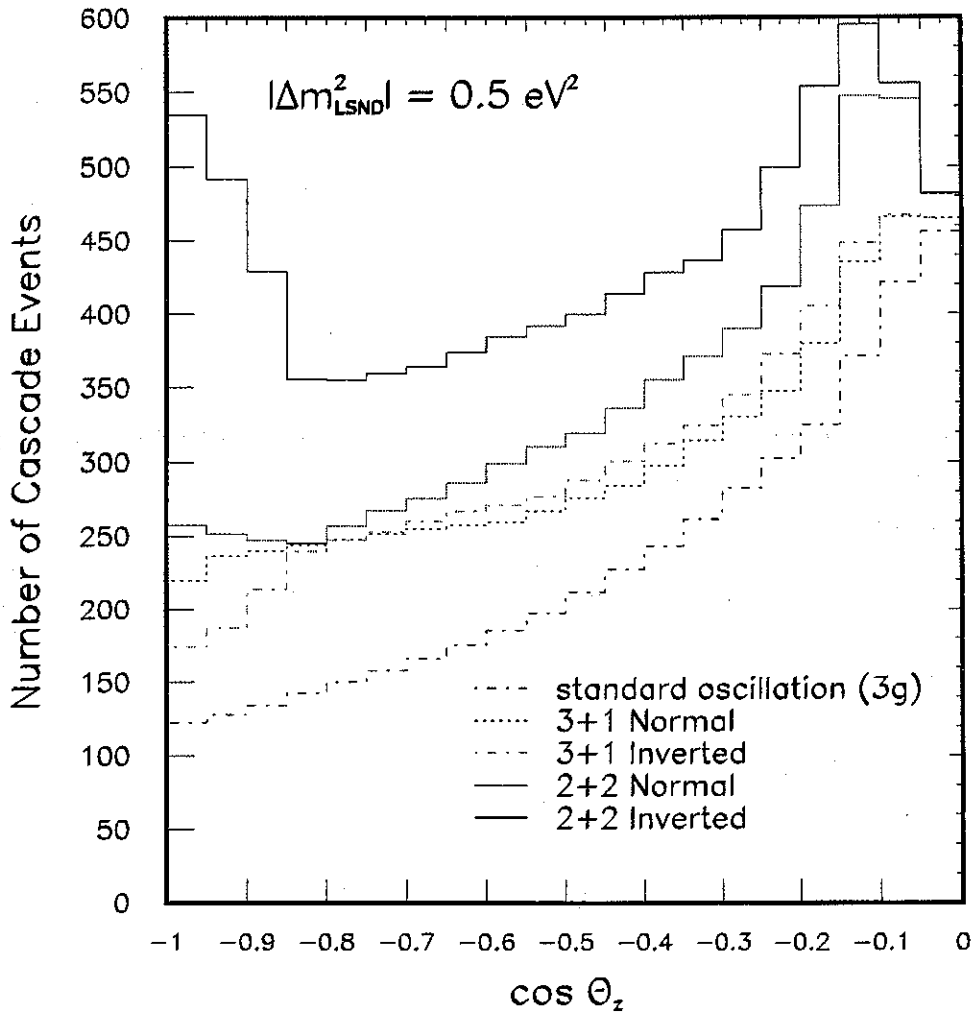

FIG. 5: Expected zenithal distribution of cascade events in the IceCube experiment after one year of data taking for the standard three flavor oscillations (3g) and the different four neutrino mass schemes.

Also, the shape of the event distributions, here the key point in disentangling the different signals, is not very much affected by the overall flux normalization.

IV. CONCLUSIONS

We have studied the rôle that can be played by a large mass splitting implied by the LSND signal, $|\Delta m^2_{\rm LSND}| \sim (0.5 - 2.0)$ eV^2 in a four neutrino mass scheme for atmospheric neutrino data in the energy range ~ 1 TeV. We have shown that upward-going muon events as well as cascade events, that can be measured by a kilometer scale detector such as the one proposed by the IceCube collaboration, can indicate the presence of the fourth neutrino through the production of $\nu_e, \bar{\nu}_e$ and $\nu_\tau, \bar{\nu}_\tau$ which are not expected in the standard three generation oscillation case where we have only the small mass splittings $\Delta m^2_\odot$ and $\Delta m^2_{\rm ATM}$. Furthermore the zenithal dependence of cascade events is even sensitive to the sign of $\Delta m^2_{\rm LSND}$ because the matter effect play an important rôle, leading to resonant $\nu_\mu \to \nu_e$ or $\bar{\nu}_\mu \to \bar{\nu}_e$ conversion depending on the sign of $\Delta m^2_{\rm LSND}$. We note that the standard three generation oscillation scheme cannot induce these signals of ν_e/ν_τ appearance at the 1 TeV scale, and therefore, they constitute an unique signature of a large mass scale present in a four neutrino mass scheme.

A final remark. If MiniBooNE observes a positive signal, the effects shown here should be expected independent of the four neutrino mass scheme. On the other hand, if MiniBooNE results turns out to be negative this may be viewed as a complementary test of the presence of a large neutrino mass splitting in nature.

Acknowledgments

This work was supported by Fundação de Amparo à Pesquisa do Estado de São Paulo (FAPESP), Conselho Nacional de Ciência e Tecnologia (CNPq), Fundo de Apoio ao Ensino e à Pesquisa (FAEP) and by the National Science Foundation under Grant No. PHY99-07949. We thank T. Stanev for providing the table of the atmospheric neutrino fluxes. We also thank C. Lunardini for bringing to our attention Ref. [17] and A. de Gouvea for useful comments. We are grateful for the hospitality of the Kavli Institute for Theoretical Physics, of the University of California in Santa Barbara, where this work was completed.

---

[1] M. C. Gonzalez-Garcia, arXiv:hep-ph/0211054.
[2] H. Nunokawa, W. J. C. Teves and, R. Zukanovich Funchal, arXiv:hep-ph/0212202 and references therein.
[3] K2K Collaboration, S. H. Ahn *et al.*, Phys. Lett. B **511** (2001) 178; M. H. Ahn *et al.*,Phys. Rev. Lett. **90**, 041801 (2003).
[4] KamLAND Collaboration, K. Eguchi *et al.*, Phys. Rev. Lett. **90**, 021802 (2003).
[5] T. K. Gaisser and M. Honda, Annu. Rev. Nucl. Part. Sci. **52**, 153 (2002).
[6] D. Hooper, H. Nunokawa, O. L. G. Peres and R. Zukanovich Funchal, Phys. Rev. D **67**, 013001 (2003).
[7] LSND Collaboration, C. Athanassopoulos *et. al.* Phys. Rev. Lett. **77**, 3082 (1996); *idem.*, Phys. Rev. C **54**, 2685 (1996); *idem.*, Phys. Rev. Lett. **81**, 1774 (1998).
[8] MiniBooNE Collaboration, A. Bazarko *et al.*, arXiv:hep-ex/0210020.
[9] C. Giunti, arXiv:hep-ph/0209103 and references therein.
[10] M. Maltoni, T. Schwetz, M. A. Tortola and J. W. F. Valle, Nucl. Phys. B **643**, 321 (2002).
[11] A. Strumia, Phys. Lett. B **539**, 91 (2002).
[12] R. Foot, arXiv:hep-ph/0208018; H. Pas, L. Song and T. J. Weiler, arXiv:hep-ph/0209373.
[13] L. Wolfenstein, Phys. Rev. D **17**, 2369 (1978); S. P. Mikheyev and A. Yu. Smirnov, Nuovo Cimento C **9**, 17 (1986); S. P. Mikheyev and A. Yu. Smirnov, Sov. Phys. JETP. **64**, 4 (1986).
[14] IceCube homepage: http://icecube.wisc.edu.
[15] M. C. Gonzalez-Garcia, M. Maltoni and C. Peña-Garay, Phys. Rev. D **64**, 093001 (2001); M. Maltoni, T. Schwetz and J. W. F. Valle, *ibidem.*, **65**, 093004 (2002).
[16] O. L. G. Peres and A. Yu. Smirnov, Nucl. Phys. B **599**, 3 (2001).
[17] E. K. Akhmedov, Nucl. Phys. B **538**, 25 (1998); E. K. Akhmedov, A. Dighe, P. Lipari and A. Yu. Smirnov, Nucl. Phys. B **542**, 3 (1999) and references therein.
[18] V. Agrawal, T. K. Gaisser, P. Lipari and T. Stanev, Phys. Rev. D **53**, 1314 (1996); T. K. Gaisser and T. Stanev, *ibidem.*, **57**, 1977 (1998).
[19] P. Lipari, M. Lusignoli and F. Sartogo, Phys. Rev. Lett. **74**, 4384 (1995) ; R. Gandhi, C. Quigg, M. H. Reno and I. Sarcevic, Phys. Rev. D **58**, 093009 (1998).
[20] P. Lipari and M. Lusignoli, Phys. Rev. D **57**, 3842 (1998).
[21] M. M. Guzzo, H. Nunokawa, O. L. G. Peres and R. Zukanovich Funchal, Nucl. Phys. Proc. Suppl. **87**, 201 (2000).
[22] T. K. Gaisser and T. Stanev, Phys. Rev. **D57** 1977 (1998).
[23] T. Stanev, Phys. Rev. Lett. **83**, 5427 (1999).
[24] S. Iyer, M. H. Reno and I. Sarcevic, Phys. Rev. D **61**, 053003 (2000); S. I. Dutta, M. H. Reno and I. Sarcevic, *ibidem.*, **62**, 123001 (2000).
[25] C. Distefano, D. Guetta, E. Waxman and A. Levinson, Astrophys. J. **575**, 378 (2002); arXiv:astro-ph/0207359.